

# Multi-Rank Subspace Change-Point Detection with Application in Monitoring Robotic Swarms

Jonghyeok Lee<sup>1</sup>, Yao Xie<sup>1</sup>, Youngser Park<sup>2</sup>, Jason Hindes<sup>4</sup>, Ira B. Schwartz<sup>4</sup>, and Carey Priebe<sup>2,3</sup>

<sup>1</sup>H. Milton Stewart School of Industrial and Systems Engineering, Georgia Institute of Technology, Atlanta, GA 30332

<sup>2</sup>Center for Imaging Science, Johns Hopkins University, Baltimore, MD 21218

<sup>3</sup>Department of Applied Mathematics and Statistics, Johns Hopkins University, Baltimore, MD 21218

<sup>4</sup>U.S. Naval Research Laboratory, Code 6792, Washington, DC 20375

## Abstract

We study real-time detection of low-rank changes in the covariance structure of high-dimensional streaming data, motivated by robotic swarm monitoring. Building on the spiked covariance model, we propose the Multi-rank Subspace-CUSUM (MRS-C) procedure, which extends classical CUSUM by tracking projection energy onto an estimated signal subspace. We analyze performance by characterizing the expected detection delay (EDD) under a prescribed average run length (ARL), deriving closed-form asymptotically optimal choices of the window size and drift. We further prove that MRS-C is first-order asymptotically optimal relative to the oracle Exact CUSUM, with an explicit efficiency constant that depends on heterogeneity in spike strengths. When the signal rank is unknown, we use a parallel procedure. Simulations and robotic swarm-behavior data illustrate robustness and effectiveness.

## 1 Introduction

Detecting abrupt changes in high-dimensional streaming data is a fundamental problem in many modern applications, from signal processing to finance and quality control. In many applications, an important class of changes involves the covariance structure of multivariate observations. Such structural changes often reflect the emergence or switching of correlated patterns among multiple sources. For example, the onset of a critical event in a sensor array may induce a common low-dimensional signal across sensors, shifting the covariance matrix from a baseline structure of nearly identity to one with a few dominant eigenvalues. Likewise, in swarm behavior monitoring, the collective motion of agents can lie in a low-dimensional subspace, so a sudden change in behavior manifests as a low-rank change in the observation covariance. Detecting these covariance shifts rapidly and reliably is crucial for a timely response in such systems.

The *spiked covariance* model (Johnstone, 2001) provides a tractable framework for capturing low-dimensional changes in covariance. It assumes that most of the variability is concentrated in a small number of principal components, making it particularly well suited to characterizing emerging signal subspaces. In this model, the covariance matrix consists of an identity baseline plus a low-rank component capturing the dominant subspace. Prior work has developed sequential detectors for rank-1 spike changes,

exploiting either the largest sample eigenvalue (Xie, Xie, and Moustakides, 2020) or an estimated leading eigenvector to construct CUSUM-type procedures (Xie, Moustakides, and Xie, 2018). However, real-world changes often involve multiple concurrent spikes of moderate strength, motivating a generalization to the multi-rank case. To address this, we extend the change-point detection framework to accommodate a general spiked-covariance setting with an unknown multidimensional signal subspace.

In this paper, we propose:

- A *multi-rank Subspace-CUSUM* algorithm that effectively detects covariance structure changes by tracking the projection energy of observations onto an estimated signal subspace.
- Rigorous theoretical analysis and optimality proof, establishing that the proposed procedure achieves first-order asymptotic optimality relative to the oracle Exact CUSUM. We also explicitly quantify the efficiency-loss constant arising from heterogeneity in signal strengths.
- Principled guidance for parameter selection, derived from the asymptotic analysis of the expected detection delay (EDD). We provide closed-form expressions for the asymptotically optimal sliding-window size and drift parameter, thereby minimizing detection delay for a target false-alarm rate.
- Comprehensive validation on both synthetic and real-world datasets, demonstrating that the proposed method outperforms existing baselines in multi-spike scenarios and successfully detects formation changes in robotic swarm behavior.

Compared with prior work, the main extension from Xie, Xie, and Moustakides (2020) to the current work is that we allow the rank of the signal subspace to exceed one, which is essential for applications like the swarm monitoring considered here. We follow their general subspace-tracking-based detection framework, but extend it to handle multiple significant eigenvalues through a parallel procedure. Theoretically, our results are generalized to cover arbitrary fixed ranks.

## 1.1 Related work

Early approaches to change-point detection treated covariance shifts within the classical statistical process control. Traditional Shewhart control charts and CUSUM procedures (Page, 1954) were extended to monitor changes in covariance in low-dimensional settings. For instance, Hotelling’s  $T^2$  control chart (Hotelling, 1947) can detect general mean or covariance shifts, and methods based on determinants or generalized likelihood have been used to detect known covariance changes. Also, Healy (1987) studied a multivariate CUSUM procedure for a covariance shift scaled by a constant. Similarly, Edward Jackson (1985) proposed using the determinant of the sample covariance as a univariate statistic to flag a covariance change. However, these classical techniques often assumed either that the post-change covariance was fully specified or that the number of data dimensions was modest.

More recent works have addressed covariance change detection in high-dimensional settings with unknown change-points in an offline manner. Notably, Chen and Gupta (2004) developed hypothesis tests for a change in a Gaussian covariance, using information criteria to estimate the change-point. Wang, Yu, and Rinaldo (2021) proposed a binary segmentation approach to localize multiple covariance breaks, while Avanesov and Buzun (2018) introduced a test based on differences in inverse covariance matrices. Arias-Castro, Bubeck, and Lugosi (2012) considered likelihood ratio tests for the appearance of a correlation between a specific subset of variables.

Despite these advances in offline analysis, the problem of sequentially detecting changes in covariance structure in real time remains relatively underexplored. Jiao, Chen, and Gu (2018) studied the sequential detection of a subspace switch using a CUSUM-type procedure; however, their method requires knowing the post-change subspace in advance. Recently, Dörnemann and Paul (2026) took a random matrix theory perspective to devise a hypothesis test for changes in the leading eigenvalues of a high-dimensional covariance sequence. Our work builds most directly on Xie, Moustakides, and Xie (2018); Xie, Xie, and Moustakides (2020), who introduced sequential procedures for detecting when the covariance matrix shifts to a spiked model with an unknown principal component. In particular, they proposed a sliding-window chart of the largest eigenvalue and a subspace-tracking CUSUM-type detector for a single-spike model.

Moreover, numerous methods have been developed to detect structural changes in evolving networks. Zhang, Xie, and Xie (2023) proposed a spectral CUSUM method to monitor changes in community structure by inspecting the eigen-decomposition of graph-related matrices. Peel and Clauset (2015) introduced a technique to flag shifts in the large-scale connectivity patterns of an evolving network, and Wang et al. (2017) proposed a multi-step algorithm for detecting such shifts in dynamic social networks. Marangoni-Simonsen and Xie (2014) developed a sequential approach based on a spectral CUSUM statistic for detecting the emergence of communities in networks. Sulem et al. (2024) designed a data-driven Siamese graph neural network, enabling online detection of distributional changes in a network without prior model knowledge. Wang et al. (2026) proposed an online tensor-based detection algorithm to identify changes in the latent connectivity structure across layers. Notably, Chen et al. (2023) introduced a spectral iso-mirror embedding to reduce a dynamic network series to a scalar representation, and Chen et al. (2024) demonstrated that a spectral Euclidean mirror technique can effectively localize “first-order” change-points in network evolution.

Our work is closely related to recent modeling efforts on swarm dynamics, which provide a foundation for the datasets considered here. In theoretical swarm dynamics, introducing range-dependent communication delays has been shown to induce rich bifurcation structures, such as torus bifurcations that transform periodic rotational swarming into quasi-periodic collective motion (Schwartz et al., 2020). Likewise, colliding swarms exhibit a critical coupling threshold beyond which they form a single coherent milling state instead of scattering, corresponding to a saddle-node bifurcation in the swarm-on-swarm dynamics (Hindes et al., 2021). Extending these foundations, Kamimoto, Hindes, and Schwartz (2023) demonstrated that when two swarms collide and merge into a combined milling state, their collective motion can transition from periodic to chaotic as key interaction parameters are varied.

## 2 Problem setup

In this section, we formalize two closely related formulations. In the *emerging subspace* setting, the data arrive as pure noise until an unknown time  $\tau$  when a low-dimensional spike is added to the covariance. In the *switching subspace* problem, the nominal spike shifts to an unknown direction at time  $\tau$ . Both problems are naturally modeled by a spiked covariance model (Johnstone, 2001).

In the *emerging subspace* formulation, the observations  $x_t \in \mathbb{R}^k$  follow a Gaussian distribution with identity covariance prior to the change, and a spiked covariance structure after the change:

$$\begin{aligned} x_t &\stackrel{\text{i.i.d.}}{\sim} N(0, \sigma^2 I_k), & t = 1, \dots, \tau, \\ x_t &\stackrel{\text{i.i.d.}}{\sim} N(0, \sigma^2 I_k + U \Lambda U^T), & t = \tau + 1, \tau + 2, \dots, \end{aligned} \tag{1}$$

where  $\tau$  is the unknown change-point. The matrix  $U \in \mathbb{R}^{k \times d}$  contains  $d$  orthonormal columns representing the directions of the emerging signal subspace, and  $\Lambda = \text{diag}(\lambda_1, \dots, \lambda_d) \in \mathbb{R}^{d \times d}$  is a diagonal matrix of signal strengths, with  $\lambda_1 \geq \dots \geq \lambda_d > 0$ . The scalar  $\sigma^2 > 0$  denotes the noise variance, which is assumed known, as it can be well estimated from nominal data. We define the componentwise signal-to-noise ratio (SNR) as  $\rho_i = \lambda_i/\sigma^2$  for  $i = 1, \dots, d$ .

Alternatively, in the *switching subspace* model, both the pre- and post-change covariances have low-rank spikes, but with possibly different subspaces:

$$\begin{aligned} x_t &\stackrel{\text{i.i.d.}}{\sim} N(0, \sigma^2 I_k + U_1 \Lambda U_1^T), & t = 1, \dots, \tau, \\ x_t &\stackrel{\text{i.i.d.}}{\sim} N(0, \sigma^2 I_k + U_2 \Lambda U_2^T), & t = \tau + 1, \tau + 2, \dots, \end{aligned} \quad (2)$$

Here,  $U_1, U_2 \in \mathbb{R}^{k \times d}$  are both semi-orthogonal matrices representing the pre- and post-change signal subspaces, satisfying  $U_1^T U_1 = U_2^T U_2 = I_d$ . In this setting, the baseline subspace  $U_1$  is assumed to be known *a priori* from the nominal distribution.

It is worth noting that the switching subspace model can be reduced to the emerging subspace formulation by projecting the data onto the orthogonal complement of  $U_1$ . Specifically, we can take a matrix  $Q \in \mathbb{R}^{(k-d) \times k}$  that satisfies  $QU_1 = 0$  and  $QQ^T = I_{k-d}$ , and define the projected observations

$$y_t = Qx_t \in \mathbb{R}^{k-d}, \quad t = 1, 2, \dots$$

Then, each  $y_t$  is Gaussian with pre-change covariance  $\sigma^2 I_{k-d}$  and post-change covariance  $\sigma^2 I_{k-d} + (QU_2)\Lambda(QU_2)^T$ . Here, the post-change covariance matrix has rank at most  $d$  and admits an eigendecomposition

$$(QU_2)\Lambda(QU_2)^T = U_y \Lambda_y U_y^T,$$

where  $U_y \in \mathbb{R}^{(k-d) \times r}$  has orthonormal columns,  $\Lambda_y = \text{diag}(\lambda_{y,1}, \dots, \lambda_{y,r})$  with  $\lambda_{y,j} > 0$ , and  $r \leq d$  is the effective post-change rank. In the case where  $\text{col}(U_2) \cap \text{col}(U_1) = \{0\}$ , we have  $r = d$ ; otherwise, components of  $U_2$  lying in  $\text{col}(U_1)$  are annihilated by the projection, and the effective rank is reduced.

Therefore, after projection, the post-change distribution can always be written in standard spiked-covariance form as

$$y_t \sim N(0, \sigma^2 I_{k-d} + U_y \Lambda_y U_y^T),$$

with signal subspace  $\text{col}(U_y)$  and spike strengths  $\lambda_{y,1}, \dots, \lambda_{y,r}$ . Thus, the switching subspace problem can be treated within the same analytical framework as the emerging subspace case. We note that this reduction involves a loss of information due to projection onto a lower-dimensional subspace. Nonetheless, it enables a unified, computationally efficient detection strategy applicable to both emerging and switching subspace scenarios. Accordingly, throughout the rest of this paper, we restrict attention to the emerging subspace model and develop the detection procedures and theoretical analysis in that setting, noting that the switching subspace problem can be handled via the projection-based reduction described above.

*Remark 2.1* (Geometric interpretation via principal angles). Let  $\theta_1, \dots, \theta_d \in [0, \pi/2]$  denote the principal angles between the subspaces  $\text{col}(U_1)$  and  $\text{col}(U_2)$ . Then the matrix

$$U_2^T (I - U_1 U_1^T) U_2$$

has eigenvalues  $\sin^2(\theta_1), \dots, \sin^2(\theta_d)$ . In particular, when  $\Lambda = \lambda I_d$ , the nonzero eigenvalues of the projected spike term  $(QU_2)\Lambda(QU_2)^T$  are given by

$$\lambda_{y,j} = \lambda \sin^2(\theta_j), \quad j = 1, \dots, d,$$

with those equal to zero corresponding to  $\theta_j = 0$ , i.e., directions in  $\text{col}(U_2)$  that lie in  $\text{col}(U_1)$  and are annihilated by the projection. More generally, for diagonal  $\Lambda = \text{diag}(\lambda_1, \dots, \lambda_d)$ , the projected spike strengths are the eigenvalues of

$$\Lambda^{1/2} U_2^\top (I - U_1 U_1^\top) U_2 \Lambda^{1/2},$$

which couples the original spike magnitudes with the relative orientation of the two subspaces.

## 2.1 Motivating application: robotic swarm monitoring

The emerging and switching subspace problems are directly relevant to modeling and analyzing collective dynamics in swarms. For example, consider a scenario in which a group of autonomous agents moves cohesively, forming stable formations characterized by low-dimensional subspaces in their positional and velocity data. When the swarm undergoes structural transitions such as splitting into subgroups, merging, or forming new coherent structures, the underlying covariance structure of the agents' movements changes accordingly, resulting in the emergence or shift of principal subspaces.

The rationale for modeling structural changes via low-rank covariance shifts is grounded in the intrinsic dimensionality commonly observed in real-world data. In many high-dimensional applications, including image sequences, network behaviors, and swarm trajectories, temporal dynamics typically concentrate energy in a few dominant directions, with the remaining dimensions largely capturing noise or insignificant variation. As illustrated in (Xie and Seversky, 2016, Figure 2), practical datasets often exhibit sharp transitions in spectral characteristics, where a small number of principal components abruptly emerge or vanish at a change-point. Leveraging a low-rank representation not only captures these fundamental structural patterns but also enhances sensitivity to subtle yet meaningful variations, thereby enabling quicker and more reliable change-point detection.

## 3 Multi-rank Subspace-CUSUM

Before presenting our Multi-rank Subspace-CUSUM (MRS-C), we briefly recall the classical CUSUM test proposed by Page (1954). When the pre-change and post-change densities are both known, this Exact CUSUM test is optimal for sequential change detection (Moustakides, 1986). In our setting, this would require full knowledge of the post-change signal subspace  $U$  and the spike magnitudes  $\lambda_i$ , quantities that are unavailable in practice. The Exact CUSUM is therefore an oracle benchmark. The MRS-C discussed in Section 3.2 estimates  $U$  and  $\lambda_i$  on the fly, enabling a practical procedure that approximates this oracle test.

### 3.1 Oracle benchmark: Exact CUSUM

The (Exact) CUSUM test (Page, 1954) uses the log-likelihood ratio between the post-change and pre-change densities. The CUSUM statistic is defined as the maximum of the accumulated log-likelihood ratio over all possible change-point locations up to time  $t$ :

$$S_t = \max_{1 \leq j \leq t} \sum_{i=j}^t \log \frac{f_0(x_i)}{f_\infty(x_i)},$$

where  $f_\infty(\cdot)$  and  $f_0(\cdot)$  denote the probability density functions of an observation before and after the change, respectively. Equivalently,  $S_t$  can be computed recursively as (Moustakides, 1986)

$$S_t = (S_{t-1})^+ + \log \frac{f_0(x_t)}{f_\infty(x_t)}, \quad S_0 = 0,$$

where  $x^+ = \max\{0, x\}$ . That is, at each time we add the new log-likelihood ratio and reset it to zero if the sum becomes negative. The stopping time for the CUSUM procedure is the first time  $t$  that  $S_t$  exceeds a preset threshold  $b$  chosen to control the false alarm rate:

$$T_C = \inf\{t > 0 : S_t \geq b\}.$$

Under the emerging subspace model (1) that we study in this paper, the log-likelihood ratio for an observation  $x_t$  is obtained as

$$\begin{aligned} \log \frac{f_0(x_t)}{f_\infty(x_t)} &= \log \left[ \frac{[(2\pi)^k |\sigma^2 I_k + U \Lambda U^T|]^{-1/2} \exp \left\{ -\frac{1}{2} x_t^T (\sigma^2 I_k + U \Lambda U^T)^{-1} x_t \right\}}{[(2\pi)^k \sigma^{2k}]^{-1/2} \exp \left\{ -\frac{1}{2\sigma^2} x_t^T x_t \right\}} \right] \\ &= \frac{1}{2\sigma^2} \sum_{i=1}^d \left[ \frac{\rho_i}{1 + \rho_i} (u_i^T x_t)^2 - \sigma^2 \log(1 + \rho_i) \right], \end{aligned}$$

The Exact CUSUM test statistic can thus be implemented by updating for each new sample  $x_t$  as

$$S_t = (S_{t-1})^+ + \sum_{i=1}^d \left[ \frac{\rho_i}{1 + \rho_i} (u_i^T x_t)^2 - \sigma^2 \log(1 + \rho_i) \right], \quad (3)$$

omitting the multiplicative factor  $(2\sigma^2)^{-1} > 0$ . When  $S_t$  exceeds the threshold  $b$ , we declare that a change has been detected.

Notably, the update term exhibits negative drift before the change and positive drift after the change. Indeed, letting  $\mathbb{E}_\infty[\cdot]$  denote expectation under the pre-change distribution and  $\mathbb{E}_0[\cdot]$  the expectation under the post-change distribution, one can see that

$$\mathbb{E}_\infty \left[ \log \frac{f_0(x_t)}{f_\infty(x_t)} \right] = -\frac{1}{2} \sum_{i=1}^d \left[ \log(1 + \rho_i) - \frac{\rho_i}{1 + \rho_i} \right] < 0, \quad (4)$$

while under the post change regime,

$$\mathbb{E}_0 \left[ \log \frac{f_0(x_t)}{f_\infty(x_t)} \right] = \frac{1}{2} \sum_{i=1}^d [\rho_i - \log(1 + \rho_i)] > 0. \quad (5)$$

This ensures  $S_t$  will tend to drift downwards (and stay at 0) in the absence of change, but will drift upwards after the change, as desired.

### 3.2 The MRS-C procedure

In practice, the Exact CUSUM requires *a priori* knowledge of the post-change subspace  $U$  and signal strengths  $\lambda_i$ , which is often unavailable. A straightforward generalized likelihood ratio approach would involve continuously re-estimating these parameters and plugging them into the likelihood ratio, but doing so naively at every time  $t$  would be computationally intensive. Instead, we propose the Multi-rank Subspace-CUSUM (MRS-C) procedure, which tracks an estimated signal subspace in real time and uses it to construct a scalable detection statistic.

We maintain an estimate  $\hat{U}_t \in \mathbb{R}^{k \times d}$  of the leading  $d$ -dimensional signal subspace at time  $t$ . At each time step, this estimate is obtained by forming the sample covariance matrix over a sliding window of length  $w$ ,

$$\hat{\Sigma}_t = \frac{1}{w} \sum_{i=t-w+1}^t x_i x_i^\top,$$

and extracting its  $d$  leading eigenvectors. Specifically, we let  $\hat{U}_t = [\hat{u}_{1,t}, \dots, \hat{u}_{d,t}]$  denote the matrix of unit-norm eigenvectors of  $\hat{\Sigma}_t$  corresponding to its  $d$  largest eigenvalues. Under the post-change regime,  $\hat{U}_t$  provides a plug-in estimate of the true signal subspace  $U$ .

The window length  $w$  controls the trade-off between estimation accuracy and adaptivity. Larger values of  $w$  improve subspace estimation but delay responsiveness to changes in the covariance structure. Before the change, the estimate reflects only noise fluctuations, whereas after the appearance of a low-rank spike, it progressively aligns with  $U$ . Accordingly, the choice of  $w$  directly affects the detection delay and must be balanced against the desired false-alarm performance.

When estimating the signal subspace at each time step, we deliberately avoid using past observations and instead construct the estimate from the next  $w$  samples. This future-window strategy has a key advantage that it ensures that the subspace estimate formed from  $\{x_{t+1}, \dots, x_{t+w}\}$  is independent of the current observation  $x_t$ , which greatly simplifies the drift calculations and theoretical analysis presented later.

Given such a delayed subspace estimate  $\hat{U}_{t+w}$  computed over the time interval  $[t+1, t+w]$ , we quantify how “signal-like” the current observation  $x_t$  is through a scalar increment  $Z_t$ . A natural choice is the squared norm of the projection of  $x_t$  onto the estimated subspace,

$$Z_t = \|\hat{U}_{t+w}^T x_t\|^2 = \sum_{i=1}^d (\hat{u}_{i,t+w}^T x_t)^2. \quad (6)$$

Here,  $Z_t$  represents the energy of  $x_t$  in the top- $d$  principal directions inferred from the future window of  $w$  observations.

Accordingly, we define the MRS-C statistic  $S_t^{\text{sub}}$  recursively as

$$S_t^{\text{sub}} = (S_{t-1}^{\text{sub}})^+ + Z_t - \Delta, \quad S_0^{\text{sub}} = 0. \quad (7)$$

The drift parameter  $\Delta$  should be set between the typical values of  $Z_t$  under the pre-change and post-change scenarios. Formally, we require the double inequality

$$\mathbb{E}_\infty[Z_t] < \Delta < \mathbb{E}_0[Z_t], \quad (8)$$

so that  $S_t^{\text{sub}}$  has a negative drift before the change and a positive drift after the change. Selection of the drift will be discussed rigorously in Section 4.1. The detection time is

$$T^{\text{sub}} = \inf\{t : S_t^{\text{sub}} \geq b\} + w \quad (9)$$

for a threshold  $b$  calibrated via Monte-Carlo simulation to achieve the desired false alarm rate. The extra “ $+w$ ” term reflects the fact that the statistic at time  $t$  is based on a subspace estimated from the future window of length  $w$ .

The MRS-C procedure, therefore, involves a trade-off between subspace-estimation accuracy and detection speed. Before the procedure can reliably raise an alarm, the delayed estimate  $\hat{U}_t$  must capture the new spike directions. This estimation window introduces an inherent delay after the true change-point during which  $\hat{U}_t$  is converging to  $U$  and  $S_t^{\text{sub}}$  may not yet be growing. Once  $\hat{U}_t$  sufficiently approximates  $U$ , the statistic adds increments  $Z_t - \Delta$  with positive mean, and thereafter  $S_t^{\text{sub}}$  behaves similarly to the Exact CUSUM.

## 4 Theoretical analysis

This section develops the theoretical performance guarantees for the proposed MRS-C procedure under the emerging subspace model. We first characterize the mean behavior of the detection statistic before and after the change, which leads to principled choices of the drift parameter and the window length. Building on these results, we derive asymptotic expressions for the EDD under a prescribed ARL constraint and establish first-order asymptotic optimality relative to the oracle Exact CUSUM.

### 4.1 Drift parameter

In this subsection, we analyse the drift parameter  $\Delta$  of the detection statistic under the rank- $d$  spiked covariance model. Recall that the statistic is updated at each time step by adding the quantity  $Z_t - \Delta$ , with a reset to zero whenever the cumulative sum becomes negative. To ensure correct operation of the procedure,  $\Delta$  must lie strictly between the pre-change and post-change expectations of  $Z_t$ . Accordingly, our main task is to characterize  $E_\infty[Z_t]$  and  $E_0[Z_t]$  under the two regimes.

Importantly, by our procedure design, the subspace estimate  $\hat{U}_{t+w}$  is computed from a moving window that does not include the current sample  $x_t$ . This ensures the independence of  $\hat{U}_{t+w}$  and  $x_t$ , which allows us to simplify the expectation as

$$\mathbb{E}Z_t = \mathbb{E}[\mathbb{E}[Z_t | \hat{U}_{t+w}]] = \mathbb{E}\left[\text{tr}\left[\hat{U}_{t+w}^T \mathbb{E}[x_t x_t^T] \hat{U}_{t+w}\right]\right].$$

**Pre-change increment.** Before the change,  $x_t$  follows  $N(0, \sigma^2 I_k)$  with no signal component. Since  $\mathbb{E}[x_t x_t^T] = \sigma^2 I_k$  and  $\hat{U}_{t+w}$  is semi-orthogonal, we have exactly

$$\mathbb{E}_\infty Z_t = d\sigma^2. \quad (10)$$

**Post-change increment.** To specify the post-change increment, we utilize the asymptotic properties of the sample eigenvectors. Throughout Section 4, we impose the following assumption for theoretical analysis.

**Assumption 4.1.** Assume the following for the true subspace covariance structure.

- (i) The subspace dimension  $d$  remains a constant.
- (ii) The population eigenvalues  $\{\lambda_i : i = 1, \dots, d\}$  are distinct and are ordered as  $\lambda_1 > \dots > \lambda_d > 0$ .

Under Assumption 4.1, each sample eigenvector  $\hat{u}_{i,t+w}$  is approximately Gaussian distributed around the true eigenvector  $u_i$ , with covariance scaling as  $w^{-1}$  (Anderson, 1963; Paul, 2007). Based on this approximation, we derive the following expression for the post-change mean of the increment. A detailed derivation can be found in Appendix A.

*Remark 4.2* (Eigenvalue multiplicity). Assumption 4.1(ii) requires distinct spike eigenvalues. This condition is imposed for proof convenience in the eigenvector perturbation arguments. The proposed detection statistic depends only on the estimated rank- $d$  signal subspace through the projection matrix, rather than on the ordering of individual eigenvectors. Consequently, the procedure remains well-defined when the spikes have multiplicity, as in several of our simulation settings in Section 6.

**Lemma 4.3** (Post-change increment). *Under Assumption 4.1, the expected increment under the post-change regime is given by, as  $w \rightarrow \infty$ ,*

$$\mathbb{E}_0[Z_t] = \sigma^2 \sum_{i=1}^d (1 + \rho_i) - \frac{(k-d)\sigma^2}{w} \sum_{i=1}^d \frac{1 + \rho_i}{\rho_i} + o\left(\frac{1}{w}\right). \quad (11)$$

Again, for the MRS-C procedure to function as intended, the drift parameter  $\Delta$  must satisfy the condition (8). Comparing the expectations, we can specify a condition for the window size  $w$  to ensure  $\mathbb{E}_0[Z_t] > \mathbb{E}_\infty[Z_t]$  by requiring the signal term to dominate the estimation error term:

$$w > \frac{k-d}{\sum_{i=1}^d \rho_i} \sum_{i=1}^d \frac{1 + \rho_i}{\rho_i}.$$

Under this condition,  $\Delta$  can take any value in the valid range.

In practice, the exact signal strengths  $\{\lambda_i\}$  may not be known in advance. However, we can design  $\Delta$  based on a conservative lower bound for the signal strength. For example, suppose it is known that each signal component has SNR at least  $\rho_{\min} = \lambda_{\min}/\sigma^2$ . A robust choice is to set  $\Delta$  to the midpoint between the pre-change expectation and a conservative estimate of the post-change expectation as

$$\Delta = d\sigma^2 + \frac{1}{2}d\lambda_{\min} = d\sigma^2 \left(1 + \frac{1}{2}\rho_{\min}\right).$$

This choice guarantees  $\mathbb{E}_\infty Z_t < \Delta$  immediately. Furthermore, provided that  $w$  is chosen sufficiently large to satisfy the condition above, it also ensures  $\Delta < \mathbb{E}_0 Z_t$ , thereby enabling effective detection even in the worst-case scenario where signal strengths are minimal.

*Remark 4.4.* Equation (11) shows that the leading term in the post-change expectation depends only on the noise level  $\sigma^2$ , the signal-to-noise ratios  $\rho_i$ , and the window size  $w$ . Importantly, this term is independent of the specific orientation of the signal subspace  $U$ . Therefore, to estimate  $\mathbb{E}_0[\|\hat{U}^T x_t\|^2]$  in practice, one may simulate the Gaussian samples using a randomly generated semi-orthogonal matrix  $U_0 \in \mathbb{R}^{k \times d}$  and covariance  $\sigma^2 I_k + U_0 \Lambda U_0^T$ .

## 4.2 Asymptotic EDD and oracle efficiency

In this section, we establish the asymptotic optimality properties of the proposed MRS-C procedure. Building on the drift analysis in Section 4.1, we derive asymptotic expressions for the EDD as the ARL tends to infinity. We then identify asymptotically optimal choices of the threshold  $b$ , drift  $\Delta$ , and window length  $w$  that minimize the detection delay, and show that the resulting performance matches that of the oracle Exact CUSUM up to a multiplicative efficiency constant.

The following Proposition 4.5 provides an explicit asymptotic characterization of the EDD for the MRS-C procedure. The result follows the classical nonlinear renewal framework for sequential change-point procedures (Tartakovsky, Nikiforov, and Basseville, 2014, Chapter 3).

**Proposition 4.5** (First-order optimal EDD for arbitrary window length). *For a prescribed ARL level  $\mathbb{E}_\infty[T^{\text{sub}}] = \gamma > 1$ , as  $\gamma \rightarrow \infty$ , if we select the threshold  $b$  and the drift  $\Delta$  as*

$$b = \frac{2\sigma^2 \log \gamma (1 + o(1))}{1 - \frac{d}{A}}, \quad (12)$$

$$\Delta = \frac{d\sigma^2}{1 - \frac{d}{A}} \log\left(\frac{A}{d}\right), \quad (13)$$

where  $A = A(w)$  represents the dominant term of the post-change increment expectation as

$$A := \sum_{i=1}^d (1 + \rho_i) \left(1 - \frac{k-d}{w\rho_i}\right), \quad (14)$$

then the EDD under the alternative is given by

$$\mathbb{E}_0[T^{\text{sub}}] = \frac{2 \log \gamma (1 + o(1))}{A - d(1 + \log(\frac{A}{d}))} + w. \quad (15)$$

In particular, Proposition 4.5 identifies a pair  $(b, \Delta)$  that asymptotically equalizes the exponential overshoot distribution under the pre-change measure. The condition  $\mathbb{E}_\infty[e^{\delta_\infty(Z_t - \Delta)}] = 1$  determines the so-called *adjustment coefficient*  $\delta_\infty$ , a standard object in nonlinear renewal theory, ensuring that the stopping rule behaves like a first-order optimal CUSUM under the nominal distribution. The detailed proof is given in Appendix A.

The expression for  $A$  in (14) represents the leading-order post-change drift of the statistic, incorporating both the spike strengths  $\{\rho_i\}$  and the window-induced eigenvector estimation error at order  $1/w$ . The asymptotically optimal delay in (15) is decomposed into two components: the intrinsic information-theoretic delay, and the estimation lag  $w$  due to the sliding window needed to estimate the evolving subspace independently. The intrinsic delay scales logarithmically with the ARL, as in the classical CUSUM theory.

Minimizing the EDD expression in Proposition 4.5 with respect to the window length  $w$  yields the optimal parameters.

**Corollary 4.6** (Optimal parameters). *To minimize the expected detection delay, the asymptotically optimal window size  $w^*$  is given by*

$$w^* = \sqrt{\log \gamma} \cdot \frac{\sqrt{2(k-d) \left(\sum_{i=1}^d \frac{1+\rho_i}{\rho_i}\right) \left(\frac{\sum_{i=1}^d \rho_i}{\sum_{i=1}^d (1+\rho_i)}\right)}}{\sum_{i=1}^d \rho_i - d \log\left(\frac{1}{d} \sum_{i=1}^d (1+\rho_i)\right)} (1 + o(1)). \quad (16)$$

Hence, corresponding optimal choice of the threshold  $b$  and the drift  $\Delta$  are given by

$$b \asymp \frac{2\sigma^2 \log \gamma}{1 - \frac{d}{A(w^*)}}, \quad \Delta = \frac{d\sigma^2}{1 - \frac{d}{A(w^*)}} \log\left(\frac{A(w^*)}{d}\right). \quad (17)$$

Finally, we establish the efficiency of our procedure relative to the oracle Exact CUSUM.

**Theorem 4.7** (First-order asymptotic optimality). *The ratio of the expected detection delays of the MRS-C ( $T^{\text{sub}}$ ) to the oracle Exact CUSUM ( $T_C$ ) is given by*

$$\frac{\mathbb{E}_0[T^{\text{sub}}]}{\mathbb{E}_0[T_C]} = \mathcal{K} + O\left(\frac{1}{\sqrt{\log \gamma}}\right), \quad (18)$$

where the efficiency constant  $\mathcal{K} \geq 1$  is defined as

$$\mathcal{K} = \frac{\sum_{i=1}^d [\rho_i - \log(1 + \rho_i)]}{\sum_{i=1}^d [\rho_i - \log(1 + \bar{\rho})]} \geq 1, \quad (19)$$

with  $\bar{\rho} = \frac{1}{d} \sum_{i=1}^d \rho_i$  representing the average signal-to-noise ratio. The constant  $\mathcal{K}$  attains its minimum value of 1 if and only if all signal strengths are uniform (i.e.,  $\rho_i = \bar{\rho}$  for all  $i$ ).

*Remark 4.8* (Difference from rank-one case). Our theoretical results generalize and unify the findings from prior studies on subspace and network change detection. First, Xie, Xie, and Moustakides (2020); Xie, Moustakides, and Xie (2018) address the rank-1 spiked covariance model. Our multi-rank framework naturally encompasses their result as a special case. When  $d = 1$ , the efficiency constant  $\mathcal{K}$  trivially becomes 1, recovering their finding that subspace tracking achieves full oracle efficiency asymptotically in the rank-1 setting. However, for  $d > 1$ , our Theorem 4.7 reveals that heterogeneity in signal strengths  $\{\rho_i\}$  introduces a penalty factor  $\mathcal{K} > 1$ . Compared to Zhang, Xie, and Xie (2023), which deals with inverse covariance structure with adjacency matrices, despite the different statistical models, both methods exhibit a similar optimal window scaling of  $w^* \asymp \sqrt{\log \gamma}$ , suggesting a universal principle for window-limited CUSUM procedures involving subspace estimation. However, the specific drift terms and the efficiency constant  $\mathcal{K}$  are unique to the geometry of the spiked covariance model.

## 5 Parallel procedure for dimension selection

Throughout our discussion and analyses thus far, we have assumed that the dimension  $d$  of the underlying subspace is known. In practice, however, the true subspace dimension is typically unknown and must be estimated from data or chosen adaptively. To handle the unknown  $d$ , we now consider running multiple detection procedures in parallel across a set of candidate dimensions  $\mathcal{D} = \{d_1, \dots, d_m\}$ . Motivated by Xie and Siegmund (2013), by setting detection thresholds for each dimension individually and ensuring the overall false-alarm rate is properly controlled, the earliest detection from these parallel runs can be taken as the final decision.

Formally, for a given candidate dimension  $d_k \in \mathcal{D}$ ,  $k = 1, \dots, m$ , the single-procedure update is

$$Z_t^{(d_k)} = \sum_{i=1}^{d_k} (\hat{u}_{i,t+w}^T x_t)^2, \quad S_t^{(d_k)} = (S_{t-1}^{(d_k)})^+ + Z_t^{(d_k)} - d_k \Delta_1,$$

with  $S_0^{(d_k)} = 0$ , and in our implementation we set  $\Delta_1 = \sigma^2(1 + \rho_{\min}/2)$ , following the guideline from Section 4. Each  $S_t^{(d_k)}$  is compared against a threshold  $b^{(d_k)}$ , where each threshold  $b^{(d_k)} > 0$  is chosen to achieve the desired ARL under the pre-change distribution. We declare that the procedure associated with dimension  $d_k$  signals a change at time

$$T^{(d_k)} = \inf\{t : S_t^{(d_k)} \geq b^{(d_k)}\}.$$

The parallel stopping rule for the overall procedure is the minimum of these stopping times all candidate dimensions

$$T_{\text{mix}} = \min_{d_k \in \mathcal{D}} T^{(d_k)} = \min_{k \in [m]} \inf\{t : S_t^{(d_k)} \geq b^{(d_k)}\}. \quad (20)$$

In words,  $T_{\text{mix}}$  is the first time any one of the  $m$  parallel statistics signals a change. The index achieving the minimum in (20),  $k^* = \operatorname{argmin}_k T^{(d_k)}$ , effectively suggests an estimate of the post-change subspace dimension as

$$\hat{d} = d_{k^*}. \quad (21)$$

The rationale is that whichever candidate dimension  $d_k$  best matches the true subspace will accumulate evidence the fastest.

Under the fixed threshold regime, given the target ARL  $\gamma$ , we employ a simple and conservative Bonferroni-type union bound using the fact that

$$\mathbb{P}_\infty(T_{\text{mix}} \leq t) \leq \sum_{k=1}^m \mathbb{P}_\infty(T^{(d_k)} \leq t).$$

Therefore, each threshold  $b^{(d_k)}$  shall be calibrated to have ARL  $m \cdot \gamma$  by Monte-Carlo simulation.

## 6 Numerical experiments

We evaluate the empirical performance of the MRS-C procedure based on both synthetic and real datasets in order to assess false-alarm control, detection delay, and robustness of the parallel process.

### 6.1 Simulation study: ARL calibration and baseline comparison

We begin with synthetic experiments that assess ARL calibration and compare detection delays across competing methods under controlled parameters. We simulate sequences of  $k$ -dimensional Gaussian observations  $x_t \sim N(0, \Sigma_t)$ , where  $\Sigma_t = \sigma^2 I_k$  for  $t \leq \tau$  before an unknown change-point  $\tau$  and  $\Sigma_t = \Sigma_1$  for  $t > \tau$ . We consider several spiked covariance scenarios for  $\Sigma_1$ :

- *Rank-1 spike*:  $\Sigma_1 = \sigma^2 I_k + \lambda u u^T$ , where  $u$  is a unit-norm eigenvector. We consider both a dense spike where  $u = (1, 1, \dots, 1)^T / \sqrt{k}$  and a sparse spike where  $u = e_1 = (1, 0, \dots, 0)^T$ .
- *Rank- $d$  spike*:  $\Sigma_1 = \sigma^2 I_k + U \Lambda U^T$  with a  $d$ -dimensional orthonormal subspace  $U = [u_1, \dots, u_d]$ . We consider uniform spikes  $\Lambda = \lambda I_d$  where all  $d$  signal eigenvalues are equal, and non-uniform spikes  $\Lambda = \operatorname{diag}(\lambda_1, \dots, \lambda_d)$  with eigenvalues  $\lambda_1 > \lambda_2 > \dots > \lambda_d > 0$  of varying strength.

Table 1: Threshold  $b$  for stopping rules corresponding to ARL of 5000, calibrated by Monte-Carlo simulation:  $\Lambda = I_d$ ,  $\rho_{\min} = 0.5$ .

$w$	20		50		100	
	$b$	ARL	$b$	ARL	$b$	ARL
$k = 5, d = 2, \sigma^2 = 1$	27.54	4953.4	25.22	5024.5	23.42	5015.2
$k = 5, d = 3, \sigma^2 = 1$	25.90	4974.8	24.56	4954.5	23.55	5005.4
$k = 10, d = 2, \sigma^2 = 1$	34.62	5036.5	30.63	4966.8	27.31	5042.6
$k = 10, d = 3, \sigma^2 = 1$	33.19	4917.0	29.23	5046.5	27.35	4996.1
$k = 20, d = 2, \sigma^2 = 1$	47.65	5038.5	40.54	4955.4	34.83	4981.2
$k = 20, d = 3, \sigma^2 = 1$	44.65	5013.6	39.24	5019.0	33.49	5046.4

In our experiments, we benchmark the MRS-C against the oracle Exact CUSUM, which has full knowledge of the post-change subspace, and the Largest-Eigenvalue Shewhart Chart (Xie, Xie, and Moustakides, 2020).

Table 1 demonstrates the thresholds  $b$  for the MRS-C procedure that yield an ARL of approximately 5000 under the pre-change distribution, calibrated by Monte-Carlo simulation. We show results for several combinations of ambient dimension  $k$ , subspace rank  $d$ , and sliding window length  $w$ . In all cases, the post-change signal strength was set to  $\Lambda = I_d$  with a lower bound of componentwise SNR of  $\rho_{\min} = 0.5$ .

Figure 1 illustrates the trade-off between ARL and EDD for three online detectors under the uniform spike model with  $k = 10$ ,  $d = 2$ , and window length  $w = 50$ . Each subplot corresponds to a different noise variance of  $\sigma^2 = 2, 1, 0.5$ . Across all noise levels, the Exact CUSUM attains the smallest detection delay for any prescribed ARL, corroborating its theoretical optimality. When the signal-to-noise ratio is low (high noise), MRS-C closely tracks the oracle performance, incurring only a modest additional delay. By contrast, the Eigenvalue Shewhart chart incurs substantially larger delays under weak signals, since its one-shot decision statistic reacts slowly to small shifts. As the signal-to-noise ratio increases (low noise), the Shewhart-type chart begins to outperform MRS-C, reflecting the well-known fact that Shewhart charts excel at detecting large, abrupt changes (Montgomery, 2020).

Table 2 reports the numerical values of the EDD for each detector when its threshold is tuned to yield an ARL of 5000 under the pre-change model. We consider three ambient dimensions  $k \in \{5, 10, 20\}$  and two subspace ranks  $d \in \{2, 3\}$ , across the same three noise variances as in Figure 1. In every configuration, the Exact CUSUM attains the smallest delay, matching its oracle status. MRS-C delivers a delay that is only slightly larger, with the gap narrowing as the signal-to-noise ratio improves (i.e.  $\sigma^2$  decreases). The Largest-Eigenvalue Shewhart chart again shows substantially higher delays at low SNR, though it becomes more competitive for stronger signals. These results corroborate the trade-offs between ARL and EDD seen in Figure 1 and demonstrate that MRS-C offers a great balance between false-alarm control and rapid detection in multi-rank spiked covariance scenarios.

## 6.2 Parallel procedure with unknown subspace dimension

We next evaluate the parallel procedure proposed in Section 5 in the setting where the post-change subspace dimension is unknown. In contrast to the experiments in Section 6.1, here multiple MRS-C charts are run in parallel for candidate dimensions, and an alarm is raised when any one of them signals.

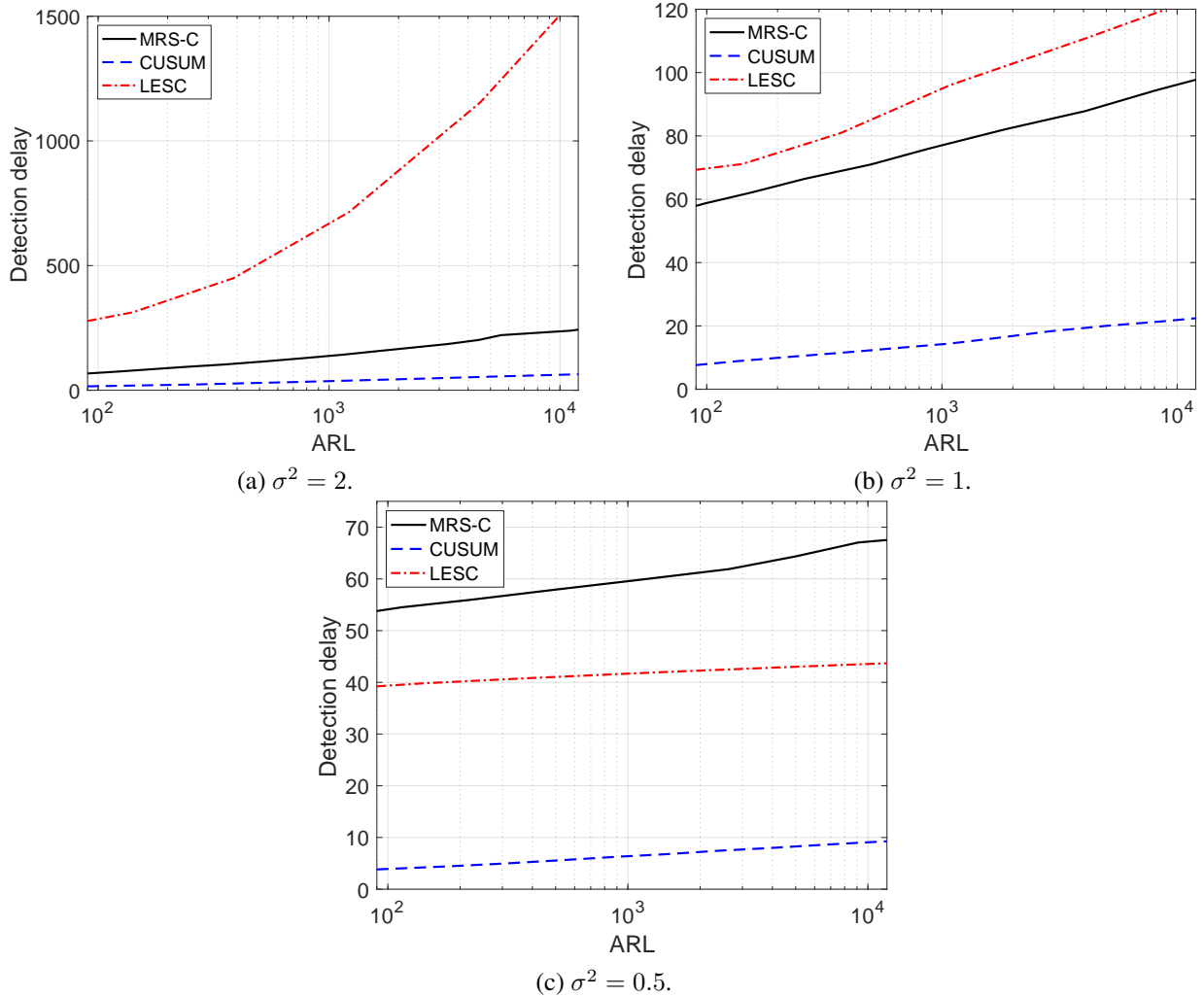


Figure 1: ARL versus EDD for three detectors under varying noise levels.

We consider the emerging subspace model in ambient dimension  $k = 20$ . Pre-change observations follow  $N(0, I_k)$ , and after the change-point fixed at  $\tau = 500$ , post-change observations follow

$$x_t \sim N(0, I_k + U_{d^*} \Lambda_{d^*} U_{d^*}^T), \quad \Lambda_{d^*} = I_{d^*},$$

where  $U_{d^*} \in \mathbb{R}^{k \times d^*}$  has  $d^*$  orthonormal columns. We fix the window length at  $w = 50$ , and the candidate dimension set is  $\mathcal{D} = \{1, 2, \dots, 10\}$ . Each individual MRS-C statistic  $S_t^{(d)}$  is assigned its own threshold  $b^{(d)}$ , calibrated individually to achieve a per-chart ARL of 50000, ensuring that the overall procedure across ten parallel charts achieves an ARL of 5000 via a Bonferroni-type argument.

The resulting thresholds calibrated by Monte-Carlo simulations and their empirical ARLs are reported in Table 3. Table 3 also summarizes rank-selection frequencies for two post-change scenarios with true ranks  $d^* = 3$  and  $d^* = 8$ . In both cases, the most frequently selected dimension matches the true post-change dimension, demonstrating that the parallel procedure can infer the latent post-change dimension

Table 2: Simulated detection delays with ARL calibrated to 5000 under  $\Lambda = I_d$ . “CUSUM” and “LESC” denote the Exact CUSUM and the Largest-Eigenvalue Shewhart Charts, respectively (standard errors in parentheses).

$k$	$d$	$\sigma^2 = 2$			$\sigma^2 = 1$			$\sigma^2 = 0.5$		
		CUSUM	MRS-C	LESC	CUSUM	MRS-C	LESC	CUSUM	MRS-C	LESC
5	2	52.9	159.6	850.2	20.1	77.1	90.6	8.4	63.7	40.1
		(0.63)	(2.70)	(20.14)	(0.12)	(0.76)	(1.67)	(0.03)	(0.09)	(0.27)
5	3	37.9	122.3	722.8	14.4	76.2	85.8	6.0	57.8	42.9
		(0.23)	(1.36)	(23.08)	(0.05)	(0.33)	(1.38)	(0.03)	(0.22)	(1.09)
10	2	52.5	196.3	1225.7	20.2	86.8	114.1	8.4	59.9	45.2
		(0.33)	(5.59)	(12.30)	(0.18)	(1.59)	(2.36)	(0.05)	(0.41)	(0.36)
10	3	38.0	153.8	1043.9	15.8	75.0	100.2	6.0	62.7	50.3
		(0.16)	(2.20)	(16.91)	(0.10)	(0.44)	(2.76)	(0.03)	(0.30)	(1.04)
20	2	52.4	349.1	2072.5	20.1	106.9	185.6	8.4	63.2	47.1
		(0.41)	(14.67)	(43.28)	(0.05)	(0.77)	(8.40)	(0.04)	(0.22)	(0.33)
20	3	38.1	247.5	1802.0	14.4	101.2	166.4	6.0	63.2	53.7
		(0.28)	(4.05)	(33.17)	(0.07)	(1.12)	(7.75)	(0.03)	(0.15)	(0.29)

Table 3: Calibrated per-dimension thresholds  $b^{(d)}$  achieving  $ARL \approx 50000$  for each candidate dimension  $d$ . The last two rows report empirical rank-selection frequencies from the parallel MRS-C procedure under two different post-change scenarios with true ranks  $d^* = 3$  and  $d^* = 8$ , respectively. In both cases, the mode of the selected dimension correctly matches the true rank.

$d$	1	2	3	4	5	6	7	8	9	10
$b^{(d)}$	40.326	43.594	44.961	46.473	46.731	47.390	48.164	48.220	48.572	48.628
ARL	50254.1	50791.2	49500.2	50096.1	49551.8	49037.4	49983.3	50477.2	49480.2	50332.0
# selected ( $d^* = 3$ )	434	840	<b>876</b>	626	495	407	331	292	234	280
# selected ( $d^* = 8$ )	48	106	177	313	375	484	696	<b>1101</b>	840	664

from the data.

Beyond identifying the true rank, the parallel strategy must also deliver competitive detection performance. We compare the proposed parallel procedure against the two fixed-rank approaches: MRS-C tuned to the true rank  $d^*$  and MRS-C detector with a misspecified dimension that fixes  $d = 1$ . The fixed-rank methods are calibrated to achieve an ARL of 5000.

Detection performance is summarized in Table 4. Across both scenarios, the parallel strategy closely tracks the detector tuned to the true rank and substantially outperforms the misspecified fixed-rank alternative. This demonstrates that uncertainty in the post-change dimension can be handled with little additional cost through the proposed parallel procedure, whereas severe rank misspecification leads to a pronounced loss of sensitivity.

The counts of false alarms before the change-point  $\tau$  in Table 4 provide an empirical measure of the effective false-alarm rate. Across both values of  $d^*$ , the parallel procedure produces substantially fewer premature alarms than the true-rank and misspecified alternatives, reflecting the conservative nature of the Bonferroni calibration. In particular, although all methods are nominally calibrated to  $ARL \approx 5000$ , the smaller number of early alarms for the parallel procedure indicates a larger effective ARL in finite samples.

Table 4: Comparison of oracle, parallel, and misspecified MRS-C procedures under true ranks  $d^* = 3$  and  $d^* = 8$ . All methods are calibrated to achieve a global ARL of 5000 under the pre-change distribution. Reported EDDs are computed over runs with  $T \geq \tau$  (standard errors in parentheses).

True rank $d^*$	Dimension selection	EDD	False alarms before $\tau$
3	True rank ( $d = 3$ )	101.80 (0.29)	429
	Parallel ( $d \in \{1, \dots, 10\}$ )	107.21 (0.45)	185
	Misspecified ( $d = 1$ )	128.62 (0.62)	399
8	True rank ( $d = 8$ )	68.24 (0.13)	448
	Parallel ( $d \in \{1, \dots, 10\}$ )	69.99 (0.12)	196
	Misspecified ( $d = 1$ )	102.15 (0.43)	392

This conservatism partially offsets the slight increase in detection delay relative to the true-rank procedure and contributes to the overall robustness of the parallel approach.

Overall, these results demonstrate that the parallel MRS-C procedure provides a robust and practically effective alternative to the true rank known detector, while avoiding the severe penalties associated with rank misspecification. The parallel procedure successfully controls false alarms and reliably detects the change without requiring prior knowledge of the true rank.

### 6.3 Robotic swarm monitoring

In this section, we qualitatively demonstrate the practical performance of the MRS-C procedure on robotic swarm datasets. We consider both a controlled synthetic swarm-trajectory dataset and a real-world UAV swarm dataset with annotated video frames. These two cases allow us to evaluate the method under complementary conditions, one in which the ground-truth change mechanisms are partially understood, and another in which changes are inferred solely from observed formation transitions.

#### 6.3.1 Synthetic milling data

We consider a synthetic swarm-trajectory dataset comprising  $T = 10001$  sequential frames of collective behavior, recorded every 0.05s over the physical-time interval 500.00-1000.00s. We index these frames as  $t = 1, \dots, T$  throughout this section. In each frame, there are  $n = 100$  agents moving in a 2D plane, and we record each agent’s two-dimensional positions  $P_t = \{p_{t1}, \dots, p_{tn}\}$  and velocity vectors  $V_t = \{v_{t1}, \dots, v_{tn}\}$ , where  $p_{ti}, v_{ti} \in \mathbb{R}^2, i = 1, \dots, n$ . Figure 2 shows a representative snapshot of the milling state at time frame  $t = 6001$ . We can construct an affinity graph, where each agent corresponds to a node, and we can observe a time series of nodal features  $\hat{X}_t = [P_t; V_t] \in \mathbb{R}^{4 \times n}$ . Let  $\tilde{X}_t$  be the position-centered and normalized nodal feature values from  $\hat{X}_t$ , which is used as the input for change-point detection algorithms after vectorization.

We compare MRS-C with two other baseline approaches, including Spectral CUSUM (Zhang, Xie, and Xie, 2023) and the iso-mirror method (Chen et al., 2023). Figure 3 illustrates the result. MRS-C yields some clearly identifiable change-points, as evidenced by a sharp rise in its detection statistic. Although ground-truth change-time labels are unavailable for this dataset, the timing of the detected change-point closely matches that of Spectral CUSUM and an independent result obtained via the iso-mirror method.

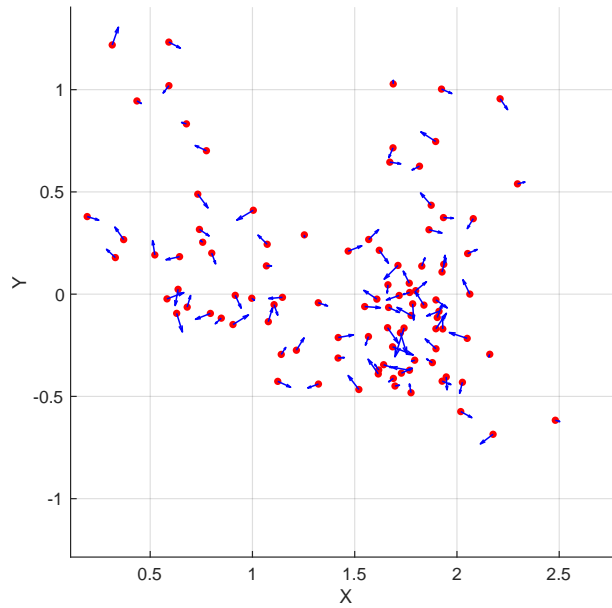


Figure 2: Snapshot of the synthetic milling swarm configuration at frame  $t = 6001$ . Red dots denote agent positions, and blue arrows indicate instantaneous velocity vectors.

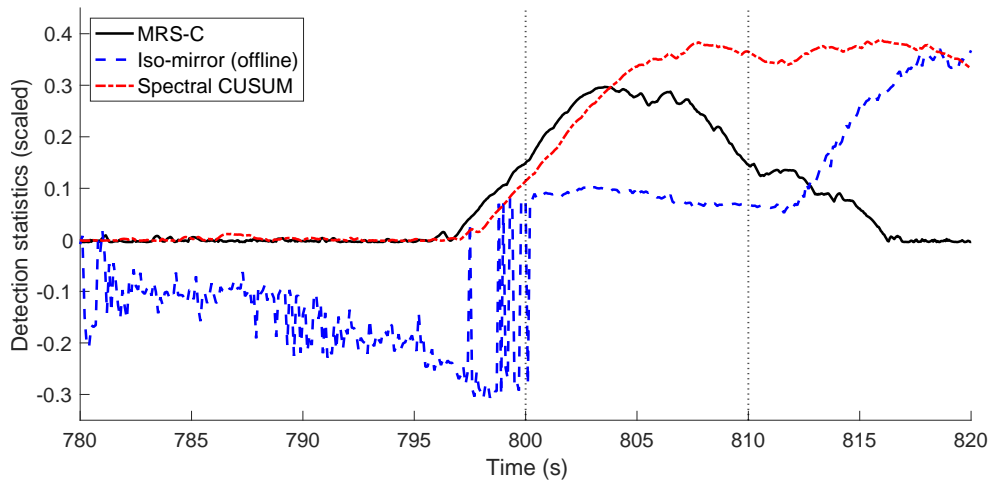


Figure 3: Detection statistics for the swarm dataset, zoomed in on the physical-time interval 780-820 s, as produced by different change-point detection methods. Both the MRS-C and iso-mirror methods identify the change-point at approximately time 800 s.

Notably, the MRS-C and the iso-mirror method are founded on entirely different statistical and algorithmic principles. We note that the iso-mirror method is an offline procedure that operates on the entire time series retrospectively, whereas MRS-C is designed for real-time sequential detection. The concordance between the detected change-points strongly suggests that both methods capture the same underlying network transition.

### 6.3.2 UAVSwarm dataset

We evaluated our method on the UAVSwarm dataset (Wang et al., 2022), which contains annotated video sequences of multiple unmanned aerial vehicles (UAVs) operating in swarm configurations under various motion patterns and environmental conditions. In particular, we used the UAVSwarm-13 sequence, which consists of 119 frames. Each frame is provided with ground-truth bounding boxes for all UAVs in view, including their object IDs, image-plane coordinates, and visibility indicators. The number of UAVs in this sequence varies across frames due to occlusions and field-of-view changes. For each frame, we extracted the center coordinates of every agent from the annotated bounding boxes, forming a structured trajectory tensor.

In the UAVSwarm-13 sequence, the UAVs initially maintain a parallel formation, flying in evenly spaced rows with stable relative positions. Around the detected change-point, several agents begin coordinated maneuvers that gradually alter the formation’s geometry. By the mid-transition stage, the swarm reconfigures into a triangular formation, with one UAV leading and others forming staggered trailing positions. Our MRS-C method clearly captures this structural transition, as evidenced by a sharp rise in the MRS-C statistic during the maneuver. Figure 4 shows representative frames and corresponding MRS-C statistics illustrating this process: before the change (parallel), during the transition, and after the new triangular formation is established.

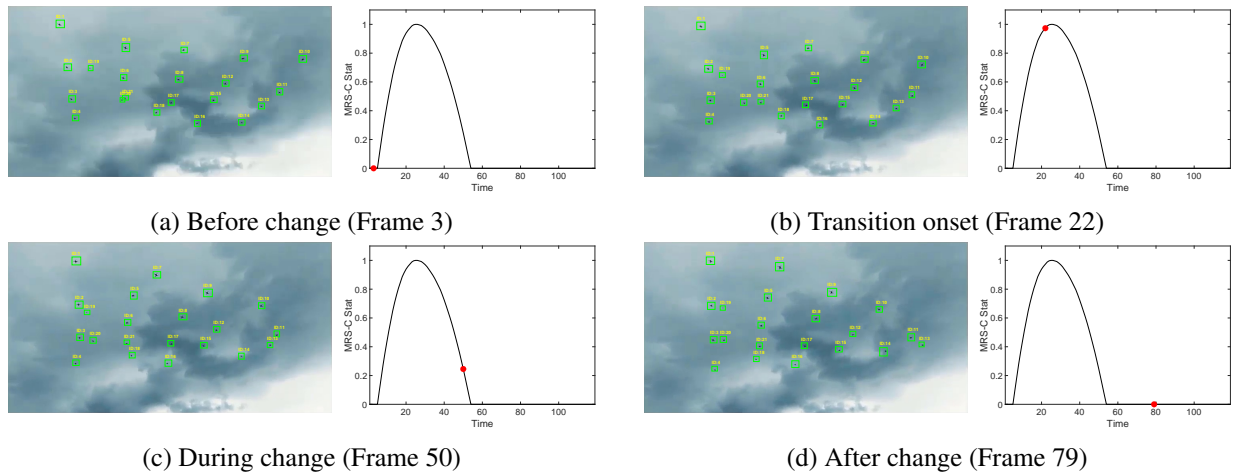


Figure 4: Illustration of swarm behavior before, during, and after the detected change-point from the UAVSwarm-13 sequence.

## 7 Conclusion

In this paper, we present the *Multi-rank Subspace-CUSUM* (MRS-C) procedure for the sequential detection of changes in covariance structure in high-dimensional streams. Our method generalizes prior subspace monitoring approaches to handle multiple concurrent spikes, thereby enhancing detection capabilities in scenarios with multiple simultaneous low-rank signals. We established a solid theoretical foundation to guide the selection of key tuning parameters that control the false-alarm rate and minimize detection delay. Analytically, we proved that the proposed detector achieves the same asymptotic order of detection delay as the oracle procedure, with a relative efficiency factor that depends on the uniformity of the signal eigenvalues. We also addressed the practical challenge of unknown subspace dimensions through a parallel monitoring scheme. Numerical experiments on synthetic data and real-world robotic swarm datasets, including UAV formations, confirmed that our method reliably achieves targeted performance and effectively captures complex structural transitions. Future work may extend this framework to non-Gaussian settings or time-varying covariances and explore adaptive strategies for dynamic subspace dimension selection.

## Acknowledgement

This work is supported by the Office of Naval Research [N000142412278]. Ira B. Schwartz and Jason Hindes were supported by the Office of Naval Research [N0001425GI101158] and NRL Base funding [N0001424WX00013].

## Disclosure of interest

No potential competing interest was reported by the authors.

## References

- Anderson, Theodore Wilbur. 1963. "Asymptotic theory for principal component analysis." *Annals of Mathematical Statistics* 34: 122–148.
- Arias-Castro, Ery, Sébastien Bubeck, and Gábor Lugosi. 2012. "Detection of correlations." *Annals of Statistics* 40: 412–435.
- Avanesov, Valeriy, and Nazar Buzun. 2018. "Change-point detection in high-dimensional covariance structure." *Electronic Journal of Statistics* 12: 3254 – 3294.
- Chen, Jie, and AK Gupta. 2004. "Statistical inference of covariance change points in Gaussian model." *Statistics* 38: 17–28.
- Chen, Tianyi, Zachary Lubbets, Avanti Athreya, Youngser Park, and Carey E Priebe. 2024. "Euclidean mirrors and first-order changepoints in network time series." *arXiv preprint arXiv:2405.11111* .

- Chen, Tianyi, Youngser Park, Ali Saad-Eldin, Zachary Lubberts, Avanti Athreya, Benjamin D Pedigo, Joshua T Vogelstein, et al. 2023. “Discovering a change point and piecewise linear structure in a time series of organoid networks via the iso-mirror.” *Applied Network Science* 8: 45.
- Dörnemann, Nina, and Debashis Paul. 2026. “Detecting spectral breaks in spiked covariance models.” *Bernoulli* 32: 1243–1266.
- Edward Jackson, J. 1985. “Multivariate quality control.” *Communications in Statistics-Theory and Methods* 14: 2657–2688.
- Healy, John D. 1987. “A note on multivariate CUSUM procedures.” *Technometrics* 29: 409–412.
- Hindes, Jason, Victoria Edwards, M Ani Hsieh, and Ira B Schwartz. 2021. “Critical transition for colliding swarms.” *Physical Review E* 103: 062602.
- Hotelling, Harold. 1947. “Multivariate Quality Control - Illustrated by the Air Testing of Bombsights.” In *Techniques of Statistical Analysis*, 111–184. McGraw-Hill.
- Jiao, Yuchen, Yanxi Chen, and Yuantao Gu. 2018. “Subspace change-point detection: A new model and solution.” *IEEE Journal of Selected Topics in Signal Processing* 12: 1224–1239.
- Johnstone, Iain M. 2001. “On the distribution of the largest eigenvalue in principal components analysis.” *Annals of statistics* 29: 295–327.
- Kamimoto, Sayomi, Jason Hindes, and Ira B Schwartz. 2023. “The chaotic milling behaviors of interacting swarms after collision.” *Chaos: An Interdisciplinary Journal of Nonlinear Science* 33.
- Marangoni-Simonsen, David, and Yao Xie. 2014. “Sequential changepoint approach for online community detection.” *IEEE Signal Processing Letters* 22: 1035–1039.
- Montgomery, Douglas C. 2020. *Introduction to statistical quality control*. John Wiley & Sons.
- Moustakides, George V. 1986. “Optimal stopping times for detecting changes in distributions.” *Annals of Statistics* 14: 1379–1387.
- Page, Ewan S. 1954. “Continuous inspection schemes.” *Biometrika* 41: 100–115.
- Paul, Debashis. 2007. “Asymptotics of sample eigenstructure for a large dimensional spiked covariance model.” *Statistica Sinica* 1617–1642.
- Peel, Leto, and Aaron Clauset. 2015. “Detecting change points in the large-scale structure of evolving networks.” In *Proceedings of the AAAI conference on artificial intelligence*, Vol. 29.
- Schwartz, Ira B, Victoria Edwards, Sayomi Kamimoto, Klimka Kasraie, M Ani Hsieh, Ioana Triandaf, and Jason Hindes. 2020. “Torus bifurcations of large-scale swarms having range dependent communication delay.” *Chaos: An Interdisciplinary Journal of Nonlinear Science* 30.
- Sulem, Déborah, Henry Kenlay, Mihai Cucuringu, and Xiaowen Dong. 2024. “Graph similarity learning for change-point detection in dynamic networks.” *Machine Learning* 113: 1–44.

- Tartakovsky, Alexander, Igor Nikiforov, and Michele Basseville. 2014. *Sequential analysis: Hypothesis testing and changepoint detection*. CRC press.
- Wang, Chuanyun, Yang Su, Jingjing Wang, Tian Wang, and Qian Gao. 2022. “UAVSwarm dataset: An unmanned aerial vehicle swarm dataset for multiple object tracking.” *Remote Sensing* 14: 2601.
- Wang, Daren, Yi Yu, and Alessandro Rinaldo. 2021. “Optimal covariance change point localization in high dimensions.” *Bernoulli* 27: 554 – 575.
- Wang, Fan, Wanshan Li, Oscar Hernan Madrid Padilla, Yi Yu, and Alessandro Rinaldo. 2026. “Multilayer random dot product graphs: Estimation and online change point detection.” *Journal of the Royal Statistical Society Series B: Statistical Methodology* 88: 282–312.
- Wang, Yu, Aniket Chakrabarti, David Sivakoff, and Srinivasan Parthasarathy. 2017. “Fast change point detection on dynamic social networks.” In *Proceedings of the 26th International Joint Conference on Artificial Intelligence, 2992–2998*.
- Xie, Liyan, George V Moustakides, and Yao Xie. 2018. “First-order optimal sequential subspace change-point detection.” In *2018 IEEE Global Conference on Signal and Information Processing (GlobalSIP)*, 111–115. IEEE.
- Xie, Liyan, Yao Xie, and George V Moustakides. 2020. “Sequential subspace change point detection.” *Sequential Analysis* 39: 307–335.
- Xie, Yao, and Lee Seversky. 2016. “Sequential low-rank change detection.” In *2016 54th Annual Allerton Conference on Communication, Control, and Computing (Allerton)*, 128–133. IEEE.
- Xie, Yao, and David Siegmund. 2013. “Sequential multi-sensor change-point detection.” In *2013 Information theory and applications workshop (ITA)*, 1–20. IEEE.
- Zhang, Minghe, Liyan Xie, and Yao Xie. 2023. “Spectral CUSUM for Online Network Structure Change Detection.” *IEEE Transactions on Information Theory* 69: 4691–4707.

## A Proofs

*Proof of Lemma 4.3.* For notational simplicity, we here denote by  $\hat{u}_i$ , instead of  $\hat{u}_{i,t+w}$ , the  $i$ -th leading unit-norm eigenvector of the sample covariance  $\hat{\Sigma}_{t+w}$ , which is the  $i$ th column of  $\hat{U}_{t+w}$ . Let  $\{u_{d+1}, \dots, u_k\}$  be an arbitrary orthonormal basis of  $\text{col}(U)^\perp$ . Under the spiked covariance model with distinct signal strengths  $\{\lambda_i\}$ , we have the following asymptotic normality of  $\hat{u}_i$ ,  $i = 1, \dots, d$  (Anderson, 1963; Paul, 2007):

$$\sqrt{w}(\hat{u}_i - u_i) \xrightarrow{d} N(0, \Xi_i), \quad (\text{A.1})$$

where the  $k \times k$  covariance matrix  $\Xi_i$  admits the spectral decomposition as

$$\Xi_i = \sum_{\substack{j=1 \\ j \neq i}}^k \frac{\mu_i \mu_j}{(\mu_i - \mu_j)^2} u_j u_j^T, \quad \mu_j = \begin{cases} \sigma^2 + \lambda_j, & j = 1, \dots, d, \\ \sigma^2, & j = d+1, \dots, k. \end{cases}$$

This  $\Xi_i$  can be rewritten as

$$\Xi_i = \frac{1 + \rho_i}{\rho_i^2} (I_k - UU^T) + \sum_{\substack{j=1 \\ j \neq i}}^d \frac{(1 + \rho_i)(1 + \rho_j)}{(\rho_i - \rho_j)^2} u_j u_j^T. \quad (\text{A.2})$$

By the eigenvector CLT (A.1), we may write

$$\hat{u}_i = u_i + \frac{1}{\sqrt{w}} \xi_i + o_p\left(\frac{1}{\sqrt{w}}\right),$$

where  $\xi_i \sim N(0, \Xi_i)$  is orthogonal with  $u_i$ . Consider the normalization map  $g(v) = v/\|v\|$ . A second-order Taylor expansion of  $g$  around a unit vector  $u$  yields

$$g(u+h) = u + (I - uu^\top)h - \frac{1}{2} \|(I - uu^\top)h\|^2 u + o(\|h\|^2).$$

Taking  $h = w^{-1/2} \xi_i$  and using  $u_i^\top \xi_i = 0$ , we obtain

$$\hat{u}_i = u_i + \frac{1}{\sqrt{w}} \xi_i - \frac{1}{2w} \|\xi_i\|^2 u_i + o_p\left(\frac{1}{w}\right).$$

Consequently,

$$\hat{u}_i \hat{u}_i^\top = u_i u_i^\top + \frac{1}{\sqrt{w}} (u_i \xi_i^\top + \xi_i u_i^\top) + \frac{1}{w} (\xi_i \xi_i^\top - \|\xi_i\|^2 u_i u_i^\top) + o_p\left(\frac{1}{w}\right),$$

and hence

$$\mathbb{E}_0(\hat{u}_i \hat{u}_i^\top) = u_i u_i^\top + \frac{1}{w} (\Xi_i - \text{tr}(\Xi_i) u_i u_i^\top) + o\left(\frac{1}{w}\right). \quad (\text{A.3})$$

From (A.2), we have

$$\text{tr}(\Xi_i) = (k-d) \frac{1+\rho_i}{\rho_i^2} + \sum_{\substack{j=1 \\ j \neq i}}^d \frac{(1+\rho_i)(1+\rho_j)}{(\rho_i - \rho_j)^2}. \quad (\text{A.4})$$

Recall that  $\hat{u}_i$  is independent with  $x_t$ . Using (A.3) and (A.4), we get

$$\begin{aligned} \mathbb{E}_0(\hat{u}_i^T x_t)^2 &= \mathbb{E}_0[\hat{u}_i^T \mathbb{E}_0[x_t x_t^T] \hat{u}_i] \\ &= \text{tr}[(\sigma^2 I_k + U \Lambda U^T) \mathbb{E}_0(\hat{u}_i \hat{u}_i^T)] \\ &= \text{tr}[(\sigma^2 I_k + U \Lambda U^T) \left\{ \frac{1}{w} \Xi_i + \left(1 - \frac{\text{tr}(\Xi_i)}{w}\right) u_i u_i^T \right\}] + o\left(\frac{1}{w}\right) \\ &= \text{tr}[(\sigma^2 I_k + U \Lambda U^T) \left\{ \frac{1+\rho_i}{w \rho_i^2} (I_k - U U^T) + \frac{1}{w} \sum_{\substack{j=1 \\ j \neq i}}^d \frac{(1+\rho_i)(1+\rho_j)}{(\rho_i - \rho_j)^2} u_j u_j^T \right. \\ &\quad \left. + \left(1 - \frac{1+\rho_i}{w \rho_i^2} (k-d) - \frac{1}{w} \sum_{\substack{j=1 \\ j \neq i}}^d \frac{(1+\rho_i)(1+\rho_j)}{(\rho_i - \rho_j)^2}\right) u_i u_i^T \right\}] + o\left(\frac{1}{w}\right) \\ &= \sigma^2 (1+\rho_i) \left\{ 1 - \frac{k-d}{w \rho_i} - \frac{1}{w} \sum_{\substack{j=1 \\ j \neq i}}^d \frac{1+\rho_j}{\rho_i - \rho_j} \right\} + o\left(\frac{1}{w}\right). \end{aligned}$$

Therefore, summing over  $i$  from 1 to  $d$ , the double sum vanishes by antisymmetry, and we obtain the expected post-change increment by

$$\begin{aligned} \mathbb{E}_0 Z_t &= \sum_{i=1}^d \mathbb{E}_0(\hat{u}_i^T x_t)^2 \\ &= \sigma^2 \sum_{i=1}^d (1+\rho_i) \left(1 - \frac{k-d}{w \rho_i}\right) - \frac{\sigma^2}{w} \sum_{i=1}^d \sum_{\substack{j=1 \\ j \neq i}}^d \frac{(1+\rho_i)(1+\rho_j)}{\rho_i - \rho_j} + o\left(\frac{1}{w}\right) \\ &= \sigma^2 \sum_{i=1}^d (1+\rho_i) \left(1 - \frac{k-d}{w \rho_i}\right) + o\left(\frac{1}{w}\right). \end{aligned}$$

□

*Proof of Proposition 4.5.* Suppose we are given the  $\delta_\infty = \delta_\infty(\Delta)$  that satisfies  $\mathbb{E}_\infty[e^{\delta_\infty(Z_t - \Delta)}] = 1$ . Then, by (Tartakovsky, Nikiforov, and Basseville, 2014, Chapter 3), as we impose the ARL  $\mathbb{E}_\infty[T^{\text{sub}}] = \gamma \rightarrow \infty$ , we have

$$\mathbb{E}_0[T^{\text{sub}}] = \frac{\log \gamma (1 + o(1))}{\delta_\infty (\mathbb{E}_0 Z_t - \Delta)} + w. \quad (\text{A.5})$$

Let  $\tilde{\Sigma} = (\sigma^{-2}I_k - 2\delta_\infty \hat{U}_t \hat{U}_t^T)^{-1}$ . Then,  $|\tilde{\Sigma}| = \sigma^{2k} / (1 - 2\sigma^2\delta_\infty)^d$  and thus

$$\begin{aligned} 1 &= \mathbb{E}_\infty [e^{\delta_\infty(Z_t - \Delta)}] = e^{-\delta_\infty \Delta} \mathbb{E}_\infty [\mathbb{E}_\infty [e^{\delta_\infty Z_t} | \hat{U}_t]] \\ &= e^{-\delta_\infty \Delta} \mathbb{E}_\infty \left[ \int_{\mathbb{R}^k} e^{\delta_\infty x_t^T (\hat{U}_t \hat{U}_t^T) x_t} \frac{e^{-x_t^T x_t / (2\sigma^2)}}{\sqrt{(2\pi)^k \sigma^{2k}}} dx_t \right] \\ &= e^{-\delta_\infty \Delta} \mathbb{E}_\infty \left[ \frac{1}{\sqrt{(2\pi)^k \sigma^{2k}}} \left( \int_{\mathbb{R}^k} |2\pi \tilde{\Sigma}|^{-1/2} e^{-x_t^T \tilde{\Sigma}^{-1} x_t / 2} dx_t \right) |2\pi \tilde{\Sigma}|^{1/2} \right] \\ &= e^{-\delta_\infty \Delta} (1 - 2\sigma^2\delta_\infty)^{-d/2}. \end{aligned}$$

Therefore, it holds that

$$\Delta = -\frac{d}{2\delta_\infty} \log(1 - 2\sigma^2\delta_\infty). \quad (\text{A.6})$$

Using Lemma 4.3 and (A.5), we get

$$\mathbb{E}_0[T^{\text{sub}}] = \frac{\log \gamma(1 + o(1))}{\sigma^2\delta_\infty A + \frac{d}{2} \log(1 - 2\sigma^2\delta_\infty)} + w. \quad (\text{A.7})$$

The denominator of (A.7) is concave with respect to  $\delta_\infty$ , so the minimizer is given as

$$\delta_\infty = \frac{1}{2\sigma^2} \left( 1 - \frac{d}{A} \right).$$

Substituting this minimizer to (A.7) and (A.6), we get (15) and (13) respectively. Also, as we assume  $w = o(\log \gamma)$ , the threshold  $b$  can be computed asymptotically as  $b = \log \gamma(1 + o(1)) / \delta_\infty$ . This results in (12).  $\square$

*Proof of Theorem 4.7.* Recall (5) that the Kullback-Leibler divergence is given by

$$\mathcal{I}_0 := \mathbb{E}_0 \log \left( \frac{f_0}{f_\infty} \right) = \frac{1}{2} \sum_{i=1}^d [\rho_i - \log(1 + \rho_i)].$$

Therefore, by the results in Tartakovsky, Nikiforov, and Basseville (2014), we have

$$\mathbb{E}_0[T_C] = \frac{\log \gamma}{\mathcal{I}_0} + O(1) = \frac{2 \log \gamma}{\sum_{i=1}^d [\rho_i - \log(1 + \rho_i)]} + O(1). \quad (\text{A.8})$$

Using the result from Proposition 4.5 and the optimal window size  $w^* \asymp \sqrt{\log \gamma}$  from Corollary 4.6, the EDD of the MRS-C is

$$\mathbb{E}_0[T^{\text{sub}}] = \frac{2 \log \gamma}{A(w^*) - d(1 + \log(\frac{A(w^*)}{d}))} + w^* + O(1),$$

and the denominator term approaches its limit

$$D^\infty := \lim_{\gamma \rightarrow \infty} \left[ A(w^*) - d \left( 1 + \log \left( \frac{A(w^*)}{d} \right) \right) \right] = \sum_{i=1}^d [\rho_i - \log(1 + \bar{\rho})],$$

with an error of order  $O(1/\sqrt{\log \gamma})$ . Therefore, the EDD for MRS-C is expanded as

$$\mathbb{E}_0[T^{\text{sub}}] = \frac{2 \log \gamma}{\sum_{i=1}^d [\rho_i - \log(1 + \bar{\rho})]} + O(\sqrt{\log \gamma}). \quad (\text{A.9})$$

Using the geometric series expansion  $(1 + x)^{-1} = 1 - x + O(x^2)$ , we get

$$\begin{aligned} \frac{\mathbb{E}_0[T^{\text{sub}}]}{\mathbb{E}_0[T_C]} &= \left( \frac{2\mathcal{I}_0}{D^\infty} + O\left(\frac{1}{\sqrt{\log \gamma}}\right) \right) \left( 1 - O\left(\frac{1}{\log \gamma}\right) \right) \\ &= \mathcal{K} + O\left(\frac{1}{\sqrt{\log \gamma}}\right). \end{aligned}$$

Since  $x \mapsto \log(1 + x)$  is strictly concave, Jensen's inequality states that

$$\frac{1}{d} \sum_{i=1}^d \log(1 + \rho_i) \leq \log(1 + \bar{\rho}).$$

Therefore,  $\mathcal{K} \geq 1$ , with equality holding if and only if all  $\rho_i$  are equal.  $\square$

## B Additional experiments

### B.1 Comprehensive simulation results

We provide comprehensive simulation results for spiked covariance scenarios mentioned in Section 6.1. Tables A.1 and A.2 are results for a rank-1 spike model with a dense and sparse signal direction, respectively. Table A.3 shows the results for a multi-rank spike model with non-uniform signal strengths.

Table A.1: Rank-1 dense spike:  $\text{ARL} = 5000$ ,  $\lambda = 1$ ,  $u = (1, 1, \dots, 1)^T / \sqrt{k}$ .

$k$	$d$	$\sigma^2 = 2$			$\sigma^2 = 1$			$\sigma^2 = 0.5$		
		CUSUM	MRS-C	LESC	CUSUM	MRS-C	LESC	CUSUM	MRS-C	LESC
5	1	90.1	211.4	550.3	35.5	97.7	136.2	14.7	65.6	57.4
		(0.84)	(3.36)	(7.53)	(0.27)	(1.98)	(1.45)	(0.13)	(0.27)	(0.28)
10	1	90.6	303.2	909.7	35.1	119.1	167.1	14.7	74.3	66.4
		(1.23)	(7.42)	(30.04)	(0.30)	(1.92)	(1.16)	(0.21)	(0.71)	(0.41)
20	1	90.5	644.1	2194.4	35.5	136.4	203.5	14.7	80.1	72.9
		(0.90)	(28.73)	(66.08)	(0.12)	(1.59)	(3.34)	(0.14)	(1.03)	(0.39)

Table A.2: Rank-1 sparse spike: ARL = 5000,  $\lambda = 1$ ,  $u = e_1$ .

$k$	$d$	$\sigma^2 = 2$			$\sigma^2 = 1$			$\sigma^2 = 0.5$		
		CUSUM	MRS-C	LESC	CUSUM	MRS-C	LESC	CUSUM	MRS-C	LESC
5	1	90.9 (0.91)	230.6 (5.44)	561.0 (5.91)	35.2 (0.39)	102.4 (2.11)	141.2 (0.43)	14.8 (0.18)	69.5 (0.52)	59.9 (0.28)
10	1	90.3 (1.12)	411.5 (8.35)	911.4 (15.25)	35.6 (0.35)	112.8 (2.07)	161.2 (0.74)	14.9 (0.24)	70.3 (0.94)	62.1 (0.30)
20	1	90.4 (1.05)	788.7 (34.20)	2255.1 (52.51)	35.4 (0.21)	145.8 (2.40)	198.4 (1.98)	14.8 (0.19)	73.0 (1.38)	68.7 (0.26)

Table A.3: Rank- $d$  non-uniform spikes: ARL = 5000,  $\Lambda = \text{diag}(\text{linspace}(2, 1, d))$ .

$k$	$d$	$\sigma^2 = 2$			$\sigma^2 = 1$			$\sigma^2 = 0.5$		
		CUSUM	MRS-C	LESC	CUSUM	MRS-C	LESC	CUSUM	MRS-C	LESC
5	2	28.6 (0.15)	90.5 (0.57)	324.7 (4.65)	11.6 (0.11)	63.9 (0.17)	67.2 (0.46)	5.3 (0.02)	56.0 (0.05)	38.9 (0.18)
5	3	20.8 (0.11)	76.9 (0.32)	256.6 (2.51)	8.4 (0.04)	61.0 (0.10)	63.8 (1.25)	3.9 (0.00)	54.2 (0.05)	35.5 (0.25)
10	2	28.5 (0.23)	109.4 (1.10)	581.1 (2.60)	11.6 (0.03)	65.5 (0.27)	76.5 (1.95)	5.3 (0.03)	56.7 (0.08)	43.2 (0.20)
10	3	20.8 (0.09)	90.9 (0.53)	403.0 (0.35)	8.3 (0.04)	59.9 (0.05)	71.2 (2.11)	3.7 (0.01)	54.5 (0.07)	40.4 (0.14)
20	2	28.5 (0.23)	153.0 (1.57)	1152.4 (9.80)	11.6 (0.08)	72.1 (0.16)	102.4 (0.72)	5.3 (0.03)	56.4 (0.16)	44.9 (0.10)
20	3	20.8 (0.06)	102.9 (1.08)	956.4 (8.11)	8.3 (0.06)	64.7 (0.08)	92.6 (0.48)	3.9 (0.02)	55.1 (0.05)	41.7 (0.28)